The University of Western Australia

Ph.D. Project Proposal

August 27, 2018

Constraining gas kinematics and distributions with spatially unresolved HI observations

Adam B. Watts

under the supervision of

Dr. Barbara Catinella
Prof. Chris Power
Dr. Luca Cortese

Abstract

Radio astronomy is entering the era of the Square Kilometre Array (SKA); and surveys with its precursors are predicted to increase the volume, resolution, and depth of observations of the cold gas in galaxies by an order of magnitude over current datasets. The majority of these data will be unresolved, in the form of a spectrum containing the combined information about the gas kinematics and distribution. This work aims to investigate the extent to which we can make statements about the distribution and kinematics of the gas in galaxies using these unresolved observations. It is essential we develop these tools now; as early science observations have already started for SKA precursor surveys. This work will utilise a combination of observational and theoretical techniques. Observational tools and datasets will be used to relate the shape of spectra to observed galaxy properties such as environment or stellar mass. Numerical simulations will be used to investigate how the shape of spectra translate to the underlying gas kinematics and distribution. Combining these methods will allow us to build connections between the properties of galaxies, the shape of their unresolved spectra, and the underlying behaviour of the gas.

Research project

Motivation and aims

Spatially resolved observations of the gaseous interstellar medium (ISM) in galaxies have shown it is a powerful tracer of galactic dynamics. Internal processes such as feedback from star formation and active galactic nuclei (Emonts et al., 2005; Boomsma et al., 2008), and external processes such as tidal interactions or ram pressure stripping from the intergalactic medium (Gunn & Gott, 1972; Kenney, van Gorkom, & Vollmer, 2004; Stevens & Brown, 2017) can impact the gas distribution and kinematics. We probe the behaviour of the gas using predominantly observations of atomic hydrogen, which traces the cold ($T < 10^4 K$) component of the ISM. However, spatially resolved observations only exist for around 500 galaxies in the local Universe (Wang et al., 2016). The majority of data are unresolved, in the form of 'global' spectra that contain combined information about the distribution and kinematics of the gas. The shape of these spectra trace the effects of the various processes of galaxy interactions and dynamics, making them a useful and more abundant tool for probing the behaviour of gas in galaxies.

The main goals of this Ph.D are understanding how the shapes of global spectra provide information about the underlying distribution and kinematics of gas in galaxies, and how they are affected by the internal and external processes of galaxy evolution. Utilising unresolved observations to their full potential is paramount as radio astronomy enters the era of the Square Kilometre Array (SKA, Dewdney et al., 2009), and its precursor instruments such as the Australian SKA Pathfinder (ASKAP) promise to map the radio sky in unprecedented resolution and sensitivity. Current surveys such as the Arecibo Legacy Fast ALFA survey (ALFALFA, Giovanelli et al., 2005; Haynes et al., 2018) produce global spectra detections on the order of $\sim 3 \times 10^4$ objects, but are restricted to the local Universe (redshift$<$ 0.06). SKA precursor surveys with ASKAP such as the Widefield ASKAP L-band Legacy All-sky Blind Survey (WALLABY, Koribalski & Staveley-Smith, 2009) and the Deep Investigation into Neutral Gas Origins (DINGO, Meyer, Heald, & Serra, 2009) are predicted to detect over half a million objects out redshift (z)= 0.25, and $\sim 3 \times 10^5$ objects to z=0.4, respectively (Duffy et al., 2012). The main data products from these surveys will be in the form of unresolved, global spectra, and early science observations for these surveys will have already started making it essential that we have the tools to exploit these datasets to their full capacity.

This work will use a combination of observational and theoretical techniques to model the shapes of global spectra. Observational datasets provide the means to draw meaningful quantification between the properties of global spectra and the other properties of galaxies. Numerical simulations of the gas disks in galaxies can be used to create mock global spectra observations which are tailored uniquely to match observational datasets, while having full knowledge of the gas behaviour. The same tools will then be applied to both datasets, providing a bridge between the shape of global spectra, the properties of galaxies, and the underlying gas dynamics.

Gas in observations

The gas in galaxies usually settles into a rotationally supported disk which is much more extended than its stellar counterpart (Bigiel & Blitz, 2012). Hydrogen constitutes 70% of the gas by mass and exists in three different phases: molecular (H_2), neutral (HI), and ionised (HII). H_2 dominates on local scales in cold ($T < 20\,K$) molecular clouds fuelling star formation, while HI is present throughout the disk and exists in a diffuse, warm ($T > 10^4 K$)

or a clumpy, cold ($T < 300\,K$) neutral medium (Field, Goldsmith, and Habing, 1969). Radio telescopes primarily detect warm HI in emission at a rest wavelength of 21.1 cm, originating from the collisionally excited electron spin-flip transition (Ewen & Purcell, 1951). As H_2 is a symmetric molecule and exists in dense cold clouds, it does not readily exhibit any emission line features. Instead it is traced using rotational emission from the carbon monoxide (^{12}CO) molecules it exists alongside, observable by radio telescopes at a rest wavelength of 2.6 mm (Dickman, 1978).

The motions of the gas throughout the disk causes a Doppler broadening of these lines, making their width a measure of the projected rotational velocity and/or the line of sight dispersion of the gas. The left panel of Fig. 1 shows the canonical 'double horn' HI emission profile exhibited by a rotation dominated galaxy, while the right panel shows the Gaussian shape typically exhibited by dispersion dominated galaxies. Gaussian profiles can be exhibited by rotation dominated galaxies if they are face on or the gas is not extended enough; as the emission is projected onto, or restricted to a narrow velocity range. The Gaussian spectrum in Fig. 1 has a host galaxy sufficiently inclined (65.3°) to show a double horn profile were it rotation dominated.

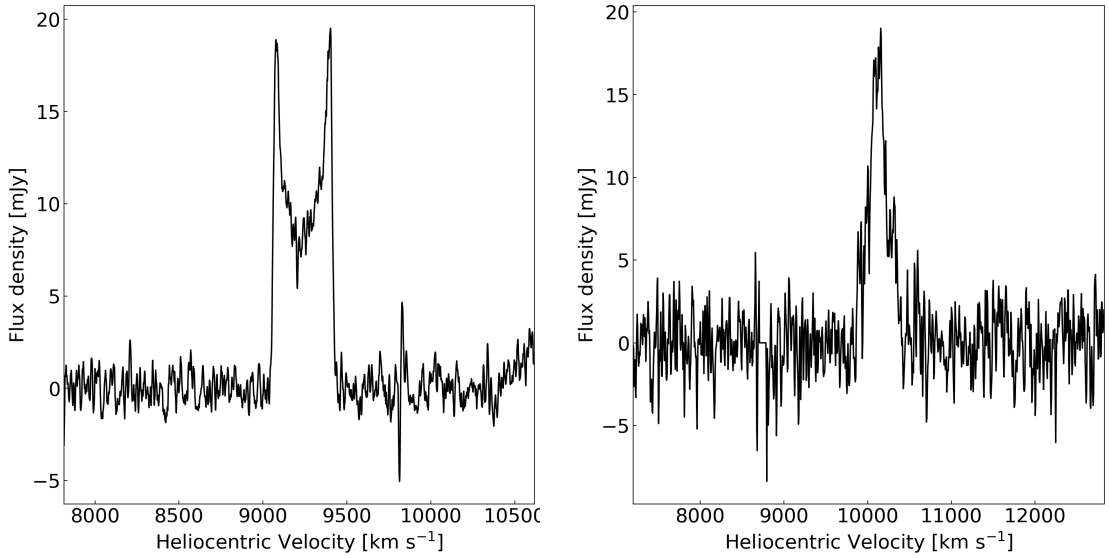

Figure 1: Left: A canonical 'double horn' HI spectrum profile shown by spiral galaxies. Right: A Gaussian-shaped HI spectrum profile shown by dispersion dominated galaxies. Spectra credit Catinella et al., (2012) and ALFALFA (Giovanelli et al., 2005).

Deviations from these relatively symmetric line profiles indicate deviations from a uniform gas distribution or ordered, regular kinematics in the galaxy. While the mass of gas hosted by a galaxy has been shown to exhibit a number of scaling relations with a galaxy's optical properties (Matthews, van Driel, & Gallagher, 1998a; Brown et al., 2018; Catinella et al., 2018), there have been few comparisons of these properties with the distribution and kinematics of the gas as traced by the shape of HI and ^{12}CO emission lines. This is one of main goals of this Ph.D; the quantitative comparison of the behaviour of the gas with galaxy properties such as environment, stellar mass, and star formation rate provides the potential to place constraints on what drives the shapes of global spectra.

Asymmetries in the optical components of galaxies have been identified in the forms of lopsided brightness distributions, spiral arms, rings, and bars (e.g., de Vaucouleurs & Freeman, 1972; Zaritsky & Rix, 1997). Further work has shown individual HI spectra are more often asymmetric than not; exhibiting double horns with differing heights and widths, edges that decline sharply or gradually, and asymmetric central troughs (Richter & Sancisi,

1994). The presence of asymmetries in spectra appear to be independent of asymmetries in the optical components of galaxies (Haynes et al., 1998; Kornreich et al., 2000), the presence of companion galaxies (Wilcots & Prescott, 2004; Ellison, Catinella, & Cortese, 2018), morphological classification (Matthews, van Driel, & Gallagher, 1998b; Espada et al., 2011), and galaxy environment (Roberts & Haynes, 1994; Matthews, van Driel, & Gallagher, 1998b; Angiras et al., 2006; Espada et al., 2011; Ellison, Catinella, & Cortese, 2018). This is shown in Fig. 2 where the left two panels show what appears to be an undisturbed spiral in the optical, but its global HI spectrum is asymmetric. Conversely the right two panels show two merging galaxies in the optical, but the global HI spectrum is symmetric. Rather than the asymmetry of individual profiles, the distribution of asymmetries as a function of galaxy properties may provide more information. Espada et al., (2011) investigated this in a sample of the most isolated galaxies in the local Universe, as they would be expected to be the least disturbed systems. They split spectra based on their width and compared the ratio of the integrated flux under the left and right sides, classifying approximately 9% to be asymmetric. This provides a baseline for comparing the rate of asymmetries in less isolated samples, and a measure of the rate of asymmetries intrinsic to gas disks that are not excited by galaxy interactions.

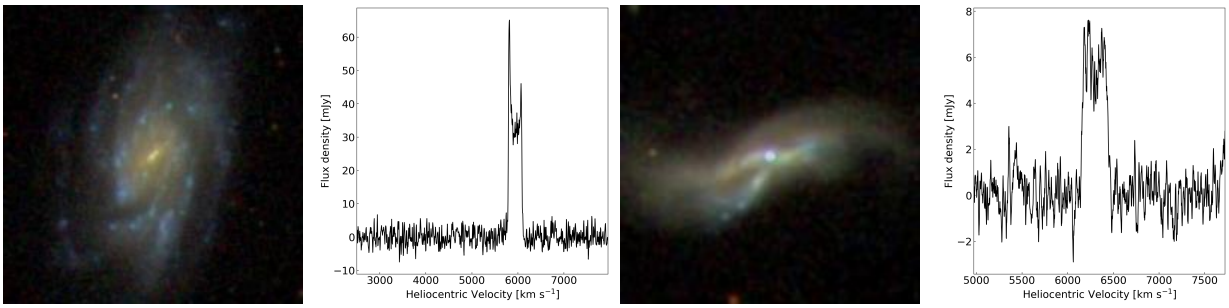

Figure 2: Examples of the difference between the optical and HI properties of galaxies. Left two panels: A spiral galaxy which appears undisturbed in the optical, but has an asymmetric HI profile. Right two panels: A visually classified post-merger galaxy which is very disturbed in the optical but has a symmetric HI spectrum. Optical image credit: SDSS, spectra from ALFALFA (Giovanelli et al., 2005) and Ellison, Catinella, & Cortese, (2018).

To gain an understanding of the shape of HI spectra we need a sample that is representative of the HI properties of galaxies in the local Universe. This has not been possible in the past, as the majority of global HI spectra are produced by blind surveys such as ALFALFA (Giovanelli et al., 2005; Haynes et al., 2018) which are biased toward gas rich galaxies. Targeted observations of global HI profiles from the extended GALEX Arecibo SDSS Survey (xGASS, Catinella et al., 2018) and ^{12}CO profiles from the extended ^{12}CO Legacy Database for GASS (xCOLD-GASS, Saintonge et al., 2017) are now available, surveys specifically designed to span a range of gas masses at a given stellar mass.

Utilising these observations is what makes this work unique, as the xGASS catalogue also contains diverse information about the galaxies such as environment and star formation rate. We hope to use this information to place the best constraints to-date on the distributions of asymmetries in global spectra.

Gas in simulations

Numerical simulations of galaxies evolve baryonic (gas and stars) and non-baryonic (dark matter) matter in time as they interact under the influence of gravity and hydrodynamics. Simulations have been used previously to investigate the drivers of asymmetries in galaxies

(e.g., Lovelace et al., 1999; Bournaud et al., 2005; Dury et al., 2008). Galaxies exhibit differential rotation, where most of the disk has the same orbital speed, and any lopsidedness would be dispersed within < 2 rotational periods (Haynes et al., 1998) due to the longer orbital time of high radii material. The high rates of asymmetric HI spectra observed in galaxy populations (50%, Haynes et al., 1998) thus imply the driving mechanism must be long lived or self-sustaining. This led authors to investigate a number of external and internal mechanisms as drivers for disk asymmetries. Lopsidedness in a perturbed disk can offset the central black hole in a galaxy, which then interacts with the disk and sustains the perturbation (Taga & Iye, 1998). Galaxy fly-by interactions inducing long-lived wakes in dark matter haloes (Weinberg, 1998), and asymmetric gas accretion (Bournaud et al., 2005) have also been suggested as mechanisms to drive disk asymmetries. Simulations contain full 6D (spatial and velocity) information, but studies commonly focus on 2D measures of optical asymmetries due to the scarcity of resolved observations of gas disks compared to optical measurements. Some work has been done quantifying the shape of gas disks from resolved observations (Holwerda et al., 2011a; Holwerda et al., 2011b), and relating these to the asymmetries of gas disks in simulations (Holwerda et al., 2011c). Though these studies only looked at the gas distribution, and focused on the identification of tidal interactions and mergers (Holwerda et al., 2011d; Holwerda et al., 2011e).

In this work we will use hydrodynamical simulations of galaxies with a modified version of the cosmological simulation code GADGET-3 (GAlaxies with Dark matter and Gas intEracT, Springel, 2005) to test the effects of perturbations in the gas disk on the shape of global HI and ^{12}CO spectra. The advantage of simulating individual galaxies using hydrodynamics is the ability to treat the gas with high resolution, allowing the detailed modelling of the shape of global profiles. Mock HI spectra have been produced from hydrodynamical simulations of galaxies recently by El-Badry et al., (2018). They measured the kurtosis of global profiles to distinguish between double horn and Gaussian shaped spectra, using this to trace whether the gas kinematics are dominated by rotation or dispersion. This only takes into account the overall shape of the profile rather than the finer details (such as the heights and widths of the peaks), and only provides insight into the overall behaviour of the kinematics at one time in the galaxy's history. The work we propose is fundamentally different. We will investigate the shape of global spectra, taking into account the peaks, trough, and wings, and how these evolve over time. This provides the connection between the effects of different perturbation events, the shape of global spectra, the underlying gas distribution and kinematics in galaxies.

Methods and current work

A number of different tools and datasets will be utilised during this Ph.D, so here we give an overview of them, how they have been applied so far, and their future scope.

Datasets

Blind surveys such as ALFALFA or the HI Parkes All-Sky Survey (HIPASS, Meyer et al., 2004) produce detections in excess of 3×10^5 objects by sweeping over large areas of the sky. However due to this strategy they are biased toward the most gas rich objects at a given stellar mass; their detection limit determined by their observation time. In order to understand how gas reservoirs vary with galaxy properties we need a sample that includes both HI rich and poor objects. The extended GALEX Arecibo SDSS Survey (xGASS, Catinella et al., 2018) is a multi-wavelength survey of 1179 galaxies over the stellar mass

range $10^9 < M_\star/M_\odot < 10^{11.5}$ with two defining features: galaxies are selected from a flat stellar mass distribution (approximately equal number of galaxies per logarithmic mass bin), and the HI observations are gas fraction limited. Selecting from a flat stellar mass distribution ensures there are enough observations of high mass galaxies to ensure good statistics; as galaxies become increasingly gas-poor with increasing stellar mass (Catinella et al., 2010; Wang et al., 2011; Lagos et al., 2011). The imposing of a gas fraction limit ($M_{\rm HI}/M_\star$) creates a sample containing systems with a range of HI masses for a given stellar mass, making it *representative* of the HI properties of galaxies. xGASS is the combination of the GASS-low and GASS surveys (Catinella et al., 2010). Respectively, they imposed gas fraction limits of 2% and 1.5% for galaxies with $M_\star > 10^{9.7}$ and $M_\star > 10^{10.5}$, and constant gas mass limits of $M_{\rm HI} = 10^8 M_\odot$ and $M_{\rm HI} = 10^{8.7} M_\odot$ for lower stellar masses. Complemented by IRAM ^{12}CO observations from xCOLD-GASS (Saintonge et al., 2017), xGASS contains the most sensitive observations of atomic and molecular gas in galaxies in the local Universe to date.

In addition to the xGASS dataset, we have a sample of 46 visually identified post-merger (PM) galaxies from Ellison, Catinella, & Cortese, (2018). Their global HI spectra observations impose the same observing strategy as xGASS, which can then act as a control sample. These PM galaxies are a valuable addition to the dataset as their interacting nature would imply they should show a high rate of asymmetries.

Modelling the shape of HI spectra

To gain a basic understanding of the shapes of HI spectra a simple model was built to produce mock single-dish observations. Using an input radial HI distribution and rotation curve (RC); moment 0 (gas surface density) and moment 1 (gas velocity) maps are produced assuming the gas is moving in purely circular orbits and exists in an infinitesimally thin disk. The moment 1 map is corrected for line of sight effects using

$$V_{\rm obs}(r, \phi, i) = V_{\rm c}(r) \cos(\phi) \sin(i) \tag{1}$$

where $V_{\rm c}(r)$ is the circular velocity at radius r, ϕ is the angle measured counter-clockwise from the receding major axis of the galaxy, and i is the inclination of the galaxy. Dispersion is added to the gas by perturbing the moment 1 map by a variate of a Gaussian with a width of $\rm V_{disp}$. Model spectra are produced by summing the contribution from pixels in the moment 0 map selected by the corresponding pixels in the moment 1 map that fall within bins of the velocity resolution $\rm V_{\mathit{res}}$. Example moment 0 and moment 1 maps are presented in Fig. 3 alongside the resulting HI spectrum.

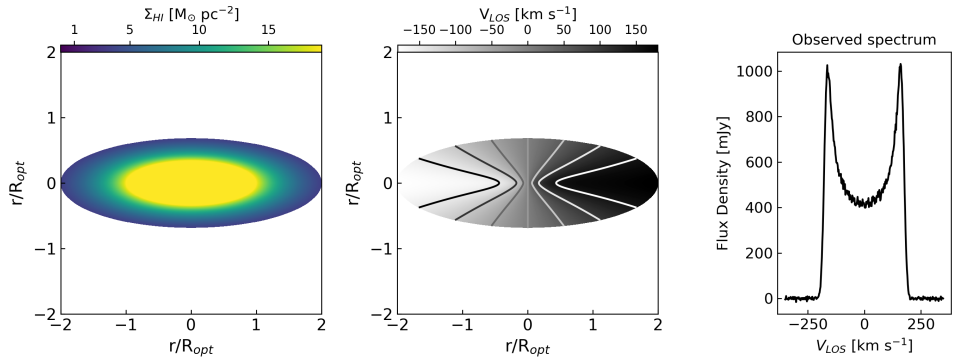

Figure 3: Model moment 0 (left) and moment 1 (middle) maps (1500 × 1500 pixels) used to create the mock spectrum (right). Contours in the moment 1 map correspond to velocity increments on the colourbar. The model assumes a distance of 10 Mpc, $i = 70°$, $\rm V_{disp} = 10$ km s^{-1}, and $\rm V_{\mathit{res}}$=2 km s^{-1}, and a 5 mJy RMS noise is added to the spectrum.

Rotation curves are selected from the templates of Catinella, Giovanelli, & Haynes, (2006), which were derived from Hα emission, as they provide a reliable parametrisation of the dynamics of disk galaxies over a range of luminosities. Various radial HI distributions can be input into the model. Interferometric maps of galaxies commonly show a flat central HI distribution within the optical radius that exponentially declines at higher radii (Leroy et al., 2008), so we favour this distribution. A constant dispersion of 10 km s^{-1} is used as this is the typical dispersion found near the optical edge of disk galaxies (Tamburro et al., 2009). The effects of different RCs and inclinations on the shape of HI spectra are shown in the top row of Fig. 4, alongside the input HI distribution and RCs. All three models have the same an input HI distribution as the blue model, which is kept as a reference. The green model has the same RC as the blue model but a lower inclination; being more face on and causing a narrower spectrum due to a loss of line of sight velocity information. The orange model has a RC that rises faster and to higher velocities than the blue model, making the observed spectrum wider and lower as the gas spans a larger range of rotational velocities.

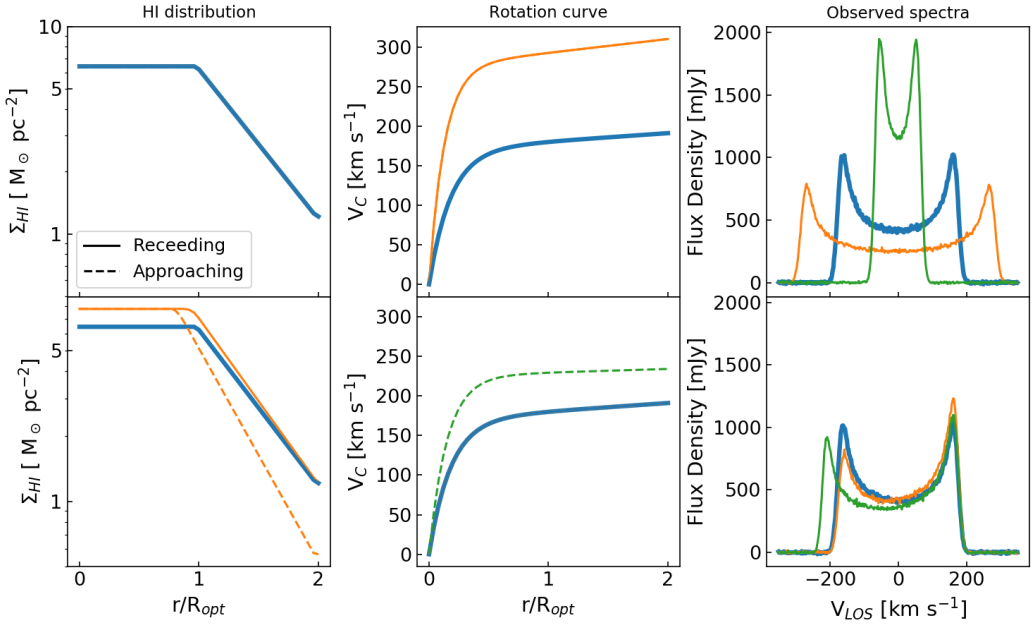

Figure 4: Symmetric and asymmetric spectra produced by the toy model. Top row: the effects of a higher RC (orange) and lower inclination (green). Bottom row: the effects of an asymmetric HI distribution (orange) and RC (green). The blue reference model is the same in both rows. All models have $M_{\rm HI} = 5 \times 10^9\, M_\odot$.

To model the asymmetries observed in HI spectra, the input HI distribution or RC parameters can be smoothly varied between the approaching (p_a) and receding (p_r) sides of the galaxy using

$$p(\phi) = p_a\left[1 + \frac{p_r - p_a}{p_a}\left(\frac{\cos\phi + 1}{2}\right)\right]. \quad (2)$$

The bottom row of Fig. 4 shows the effects of varying the HI distribution or RC between the approaching and receding sides using Eq. 2. In all three models the HI distribution and RC are the same on the receding side, and the blue model is the same symmetric blue model as shown the top row for reference. The orange model has a truncated HI distribution on the approaching side, making the height of the approaching peak lower, the receding peak higher, and the shape of the trough uneven. The green model has a RC that rises higher on its approaching side, shifting the approaching peak further from the centre and reducing its height as the HI is spread over a larger range in velocity.

Many of the xGASS spectra show asymmetry, and it is possible to reproduce their shape (to an extent) using this simple model. By matching the inclination, distance, HI mass, and centre of the model to those measured by the survey, the measured width of the spectra is used to estimate the velocity of the approaching and receding sides. Using these velocities to select appropriate RCs; editing the HI distribution lets us reproduce some of the global properties of xGASS spectra. Fig. 5 demonstrates the ability of the model to match the shape of the trough and the slope of the edges, but there is some difficulty matching the width of the peaks which are consistently too narrow in this model. A caveat in this analysis is the measured centre of the spectrum may not correspond to the true centre of velocity for the galaxy, a problem highlighted in the bottom right panel of Fig. 4. Measuring the minimum of the central trough or flux weighted centre of one of these asymmetric spectra will not yield $V_{LOS} = 0$ km s^{-1}. We therefore cannot be sure that matching these models to the centre of observed spectra will yield the correct model RCs, which in turn would cause an incorrect modelling of the HI distribution.

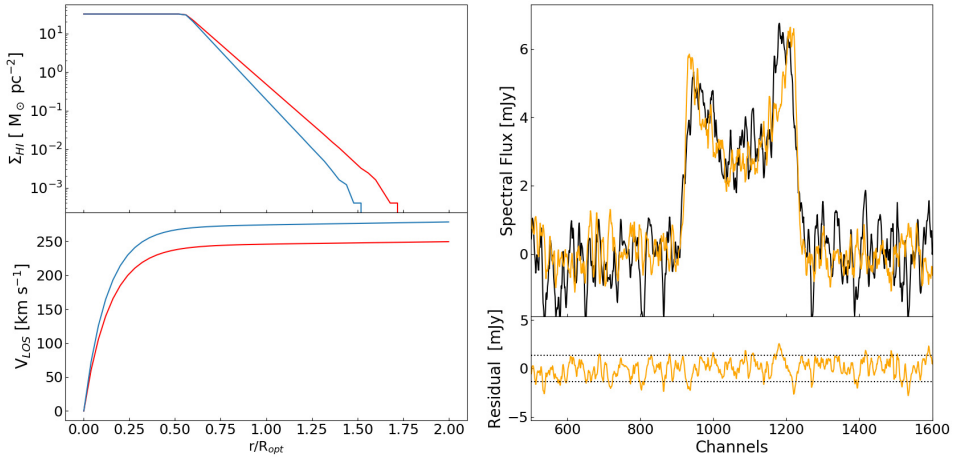

Figure 5: Input approaching (blue) and receding (red) HI distributions and RCs used to generate the model spectra (orange), matched to the xGASS spectrum (black) on the right. Black horizontal lines in the residual are the 1σ RMS noise of the observed spectra.

The HI toy model is good for understanding the basic shapes of HI profiles, but if we want to investigate what drives the asymmetries of HI spectra we need a more complex model. Hydrodynamical simulations with a modified version of the code GADGET3 (Springel, 2005) will be used to model realistic distributions of gas in galaxies under the influence of perturbations. As we are primarily interested in the gas distributions we can set up stars and dark matter, commonly modelled as particles, in an equilibrium system using the code GALIC (Yurin & Springel, 2014) and model them as a static gravitational potential. This frees up computational resources and allows the gas component to be treated with much higher resolution. Mock observations will be created from these simulations and compared to the xGASS and PM catalogues.

Measuring the shape of HI spectra

HI spectra come in a diverse range of shapes. There could be one or two peaks, a wide or narrow trough, straight or gradual edges; and these could be different on either side of the profile. Moreover spectral resolution, noise, and radio frequency interference (RFI) introduce factors that can make the shapes of profiles uncertain, especially if the signal is weak. The extraction of information from large samples of spectra needs a robust and reliable, yet versatile parametrisation of the shapes of HI profiles. Previous works (e.g.,

Saintonge, 2007; Obreschkow et al., 2009b; Obreschkow et al., 2009a) have utilised various analytical functions which have advantages such as few free parameters and the ability to describe steep edges; but are hindered due to low versatility or being undefined for certain parameter ranges. The 'busy function' developed by Westmeier et al., (2014) was designed to describe the steep edges, narrow peaks and wide troughs often observed in HI spectra.

$$B(x) = (a/4) \times (\mathrm{erf}[b_1(x - x_E)] + 1) \times (\mathrm{erf}[b_2(x - x_E)] + 1) \times (c\,|x - x_P|^N + 1) \quad (3)$$

The advantage to having an analytic description of a profile is the ability to parametrise the overall properties (e.g. width, integrated flux) as well as the finer details (e.g. slope of the edges) much easier. The busy function was fit to the HI detections in the xGASS and PM samples. It's eight free parameters makes it versatile for fitting the shapes of HI spectra, but makes it prone to erroneous outputs that can be hard to detect automatically. The presence of strong noise, RFI, or nearby gas rich companions can also cause the busy function to fit the incorrect part of the spectrum. To mitigate these problems each fit was visually inspected, and if required the fitting region was redefined or priors were provided for the fit parameters. In some cases it was necessary to force one of the parameters to prevent unrealistic values for others. This took longer than expected to implement as there were some initial issues fitting the busy function reliably. Some fits are still uncertain due to low signal to noise (S/N), uncertain HI profiles, or profile shapes that are difficult to fit; so from here we restrict our analysis to those profiles where good fits have been confirmed and have S/N > 10. This amounts to 388 of the 707 xGASS detected galaxies and 25 of the 46 PM galaxies.

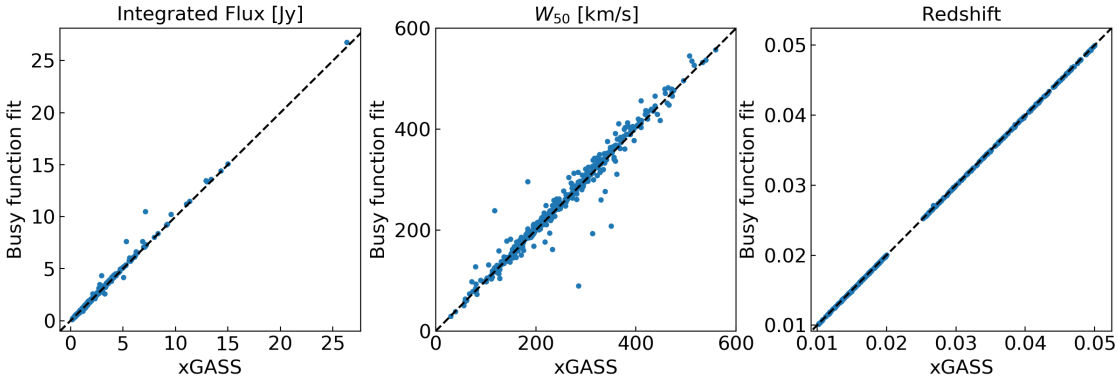

Figure 6: A comparison of measurements from the busy function fits and xGASS.

Figure 6 is a comparison of the integrated fluxes, the widths of spectra, and the cosmological redshifts of xGASS galaxies derived from the busy function fits and as measured by Catinella et al., (2018). Integrated fluxes are computed under the observed spectrum using the busy function fit to define the limits of the signal, and widths are measured at the 50% level of each peak (W_{50}) in the busy function fit. Good agreement is shown between the parameters. Outliers in the integrated flux have been visually confirmed to be small differences in the integration range defined by the fits, and outliers in the W_{50} have been identified as spectra where measurements of the peaks differ between the fit and spectrum due to noise.

Quantifying the asymmetry of HI spectra can be done visually (e.g., Richter & Sancisi, 1994), or by comparing meaningful measurements on the approaching and receding sides of the spectrum (e.g., Tifft & Cocke, 1988; Haynes et al., 1998). The areal asymmetry parameter introduced by Haynes et al., (1998) compares the ratio of the integrated flux above and below the middle velocity $V_m = (V_h + V_l)/2$, where V_l and V_h are the velocities

where the spectrum equals 20% of the highest peak on the left and right sides. The areal asymmetry parameter is then $A_{fr} = A$ or $1/A$ if $A < 1$ where

$$A = \frac{\int_{V_m}^{V_h} S_v dv}{\int_{V_l}^{V_m} S_v dv}. \tag{4}$$

We use our busy function fits to define V_l and V_r at the 20% level of the respective peaks on the left and right hand side of the spectra, or the single peak in the case of single peaked profiles. Using the fits reduces uncertainty in measuring peak heights and the locations of V_l and V_h, and using the 20% level of individual peaks rather than the highest peak (e.g., Haynes et al., 1998; Espada et al., 2011), makes A_{fr} more sensitive to spectra with gradually sloping edges or significantly different peak heights. We calculate A_{fr} by integrating under the observed spectrum, rather than the busy function fit, as this is more sensitive to smaller scale variations the busy function may average over. The effects of noise are assumed to be uniform over the profile. Due to global HI spectra being unresolved, if there are multiple galaxies in the same observation with similar recessional velocities their emission lines will overlap making them impossible to disentangle. To ensure we do not bias our measure of asymmetries we remove these confused sources from our A_{fr} calculations for now; we will investigate the asymmetries of confused spectra in the future. This leaves us with 365 xGASS galaxies with high S/N.

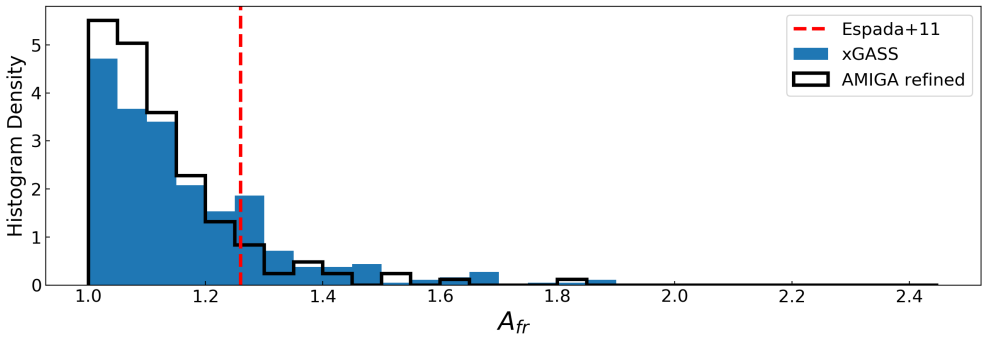

Figure 7: Comparison between the distribution of A_{fr} values in the xGASS sample (blue, filled), and the AMIGA refined subsample (black). The red dashed line corresponds to $A_{fr} = 1.26$; the AMIGA threshold for asymmetry.

In Fig. 7 we compare density normalised histograms of the distribution of flux ratio parameters from xGASS to the AMIGA refined subsample of isolated galaxies from Espada et al., (2011).The refined subsample galaxies are selected to have the lowest flux ratio uncertainties ($\Delta A_{fr} < 0.05$) to remove galaxies which could have biased asymmetry measures due to profile uncertainties. The xGASS histogram is lower and wider than refined subsample; indicating the xGASS HI profiles show both stronger and higher frequencies of asymmetries. This is expected, as the AMIGA galaxies are selected to be some of the most isolated and undisturbed galaxies in the local Universe. Espada et al., (2011) fit a half-Gaussian to the refined subsample and define the thresholds of $A_{fr} > 1.26$ (2σ) and $A_{fr} > 1.39$ (3σ) corresponding to asymmetric and strongly asymmetric profiles respectively. At the same levels, 21% of the xGASS galaxies are asymmetric and 8.5% are strongly asymmetric; compared to 9% and 5% in the refined subsample.

Galaxy environment has been suggested as a driver of asymmetries in disk galaxies (e.g., Zaritsky & Rix, 1997; Angiras et al., 2006), due to varying frequencies of tidal interactions. This would suggest that galaxies in denser environments would show larger values of A_{fr}

more frequently. In Fig. 8 we divide the xGASS galaxies into their environmental classifications and compare them, along with the PM sample, to the overall xGASS distribution as a reference for the general population. The expected trend with environment is apparent in the histograms. The isolated centrals show the narrowest A_{fr} distribution, consistent with them experiencing the least tidal interactions. The satellite galaxies show higher asymmetry rates and strengths than the isolated centrals, and the group centrals show a histogram with a peak that is shifted away from $A_{fr} = 1$. The PM galaxies show the most irregular distribution of A_{fr} values, but this may be due to the small sample size.

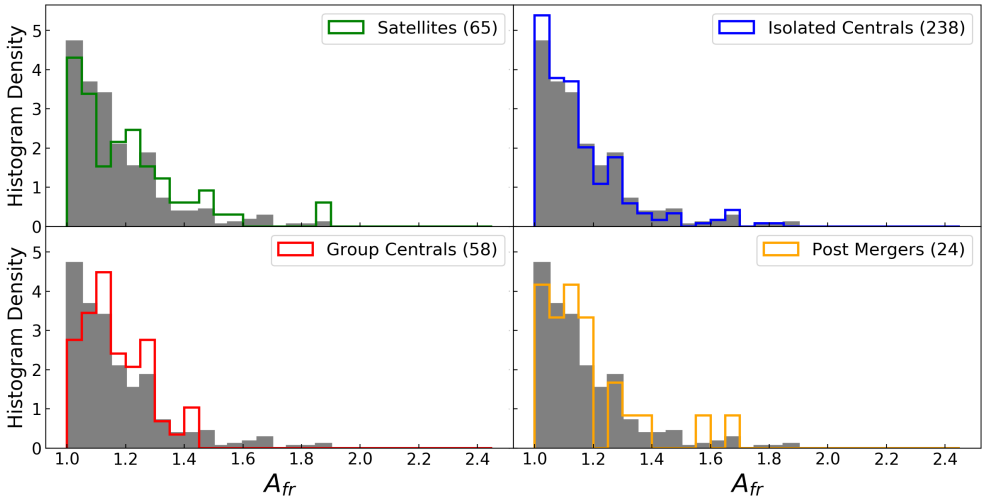

Figure 8: The distribution of A_{fr} values of xGASS and PM galaxies as a function of their environment. The number of galaxies in each subsample is indicated in the legends.

Work is in progress fitting the busy function robustly to profiles with lower S/N, and those with higher S/N but uncertain fits. This will increase the number of galaxies in the above histograms, increasing the statistics and providing better estimates of the asymmetry rates. We are also investigating the effect of the S/N of individual profiles on the value of their flux ratio parameter, and determining if we can reliably extend V_l and V_h beyond the 20% level of the peaks. As this work progresses; we are looking toward developing better measures of the asymmetry of global spectra, and methods of comparing the distributions of these parameters.

Project details

Confidential and intellectual property

My work has no intellectual property restrictions or issues accessing confidential information. The xGASS dataset and the busy function fitting algorithm are publicly available, and the PM dataset was provided by Dr. Catinella. The simulation code GADGET-3 has been provided by Prof. Power. Proper citations and credit will be given to all authors whose work or tools I use. If any of this changes I will inform the Graduate Research School.

Fieldwork information

My research will be conducted at the University of Western Australia, however there will be the possibility of travel both interstate and overseas for conferences or collaboration.

Facilities

All the facilities I require are already present at the University of Western Australia.

Approval

There are no current or foreseeable approval requirements for my research. Should I need approval in the future I will inform the Graduate Research School.

Skills audit

A self assessment of my research skills can be found in Table 1.

Table 1: Self assessment of my research skills

Research skill	Level	Desired level	Evidence	Plan
Identifying and utilising appropriate bibliographic resources	Basic	Proficient	Masters thesis and two published research papers.	I will practice by regularly reading papers and identifying sources within the works.
Use of information technology skills relevant for research	Competent	Proficient	I have experience with IDL, and Fortran with OpenMP and MPI implementation for parallel code.	I will learn new languages as necessary, and continue to develop my knowledge of Python.
Familiarity with the principles and conventions of academic writing	Basic	Proficient	Comments from my co-authors/supervisor for my masters thesis and research papers often contained feedback about writing style.	I will constantly write and receive feedback from my supervisors and fellow students and attend writing workshops.
Ability to constructively defend research outcomes at seminars and conferences	Basic	Proficient	Despite positive feedback I do not feel confident when presenting.	I will practice, attend workshops, and ensure I prepare well in advance.
Understanding and application of relevant data collection and analysis methods	Competent	Proficient	I have undertaken two research projects but often the data analysis methods had already been developed, or I had direction on how to proceed.	Through practice and consulting with my supervisors I'll build the knowledge to effectively investigate project aims using the correct methods.

Research project communication

On the 9th of August I defended my research proposal in front of a review panel and the staff and students at ICRAR. I will present yearly progress reports to the same panel and audience beginning in February 2018. My thesis is planned to be submitted as a series of papers which I outline below:

1. **A statistical quantification of the shapes and asymmetries of HI spectra** How does the shape of HI spectra vary as a function of galaxy properties? Are asymmetries more prominent in different sub samples, and what is the distribution of asymmetries in the cold gas scaling relations?
2. **Asymmetries in the cold dense medium of galaxies traced by carbon monoxide** Carbon monoxide (^{12}CO) emission traces the cold, dense molecular clouds that harbour star formation. How does the shape of ^{12}CO spectra vary with the properties of galaxies and the cold gas scaling relations?
3. **The drivers of asymmetries in galaxies probed by numerical simulations** Using hydrodynamical simulations, how do the shape of global HI and ^{12}CO spectra respond to perturbation of the gas disk? What are the strength and lifetime of the effects, and how do they depend on the properties of galaxies and the type of the perturbation?

Data management

Most of my data will be stored on the laptop provided to me by the University, and on the ICRAR computer cluster Pleiades should I need to use more powerful computing resources.

Research training

Research training plan

A time line of my research plan is provided as a GANTT chart shown in Fig. 9

Confirmation of candidature

My confirmation of candidature requires a number of tasks to be completed. I have listed these below with the expected or fulfilled completion dates.

- AACE1000 Academic Conduct Essentials: March 2012 (during undergraduate)
- UWA Ethics Approval: Not required
- Project proposal presentation - 30 minute presentation to review panel and ICRAR staff & students: 9th August 2018
- Project proposal report: 11th August 2018
- Coursework totalling 6 points - UWA/ICRAR requirement: 12th November 2018
- Annual progress report - substantial piece of writing at an adequate level: 11th February 2019
- Annual progress seminar - 30 minute presentation to review panel and ICRAR staff & students: February 2018

Working hours

I will work the required 30 hours per week at minimum.

Budget

I have been allocated $1250 from the ECM faculty for the purchase of a new laptop, $1850 from the GRS for international conference travel, and up to $3250 from ICRAR to aid with expenses. I will join the ASA which will provide $1000 in travel expenses to the ASA Harley Wood Schools and conferences. I can also apply for additional funding as an ASTRO 3D student. Table 2 contains my current and projected expenses.

Table 2: Estimated expenses during my Ph.D. Costs that are underlined have already been incurred while others are projections.

Description	Estimated cost	Funds available	Funding source
Laptop with extended hard drive	$\underline{\$1662.93}$	$1250 $412.93	ECM ICRAR
Domestic conference travel	$2000	$1000 $1000	ASA ICRAR
International conference travel	$3550	$1850 $1837.07	GRS ICRAR
Poster printing	$100	$100	ICRAR

Supervision

Principal Supervisor: Dr. Barbara Catinella [40%]
Dr. Catinella and I will meet weekly to discuss my current progress and future work. More regular meetings will be scheduled if required.

Coordinating Supervisor: Prof. Chris Power [40%]
Prof. Power and I will meet as-needed for the beginning of my Ph.D, and transition to weekly as my research becomes more numerically focused.
Cosupervisor: Dr. Luca Cortese [20%]
Dr. Cortese and I will meet as-needed, which will commonly be in conjunction with Dr. Catinella.

References

Angiras, R. A. et al. 2006. *MNRAS* 369, 1849.
Bigiel, F. & L. Blitz. 2012. *ApJ* 756, 183, 183.
Boomsma, R. et al. 2008. *A&A* 490, 555.
Bournaud, F. et al. 2005. *A&A* 438, 507.
Brown, T. et al. 2018. *MNRAS* 473, 1868.
Catinella, B. et al. 2012. *A&A* 544, A65, A65.
Catinella, B. et al. 2006. *ApJ* 640, 751.
Catinella, B. et al. 2010. *MNRAS* 403, 683.
Catinella, B. et al. 2018. *MNRAS* 476, 875.
de Vaucouleurs, G. & K. C. Freeman. 1972. *Vistas in Astronomy* 14, 163.
Dewdney, P. E. et al. 2009. *IEEE Proceedings* 97, 1482.
Dickman, R. L. 1978. *ApJS* 37, 407.
Duffy, A. R. et al. 2012. *MNRAS* 426, 3385.
Dury, V. et al. 2008. *MNRAS* 387, 2.
El-Badry, K. et al. 2018. *MNRAS* 477, 1536.
Ellison, S. L. et al. 2018. *MNRAS* 478, 3447.
Emonts, B. H. C. et al. 2005. *MNRAS* 362, 931.
Espada, D. et al. 2011. *A&A* 532, A117, A117.
Ewen, H. I. & E. M. Purcell. 1951. *Nature* 168, 356.
Giovanelli, R. et al. 2005. *AJ* 130, 2598.
Gunn, J. E. & J. R. Gott III. 1972. *ApJ* 176, 1.
Haynes, M. P. et al. 1998. *AJ* 115, 62.
Haynes, M. P. et al. 2018. *ApJ* 861, 49, 49.
Holwerda, B. W. et al. 2011a. *MNRAS* 416, 2401.
— 2011. b. *MNRAS* 416, 2415.
Holwerda, B. W. et al. 2011c. *MNRAS* 416, 2426.
Holwerda, B. W. et al. 2011d. *MNRAS* 416, 2437.
Holwerda, B. W. et al. 2011e. *MNRAS* 416, 2447.
Kenney, J. D. P. et al. 2004. *AJ* 127, 3361.
Koribalski, B. & L Staveley-Smith. 2009.
Kornreich, D. A. et al. 2000. *AJ* 120, 139.
Lagos, C. D. P. et al. 2011. *MNRAS* 418, 1649.
Leroy, A. K. et al. 2008. *AJ* 136, 2782.
Lovelace, R. V. E. et al. 1999. *ApJ* 524, 634.
Matthews, L. D. et al. 1998a. *AJ* 116, 2196.
— 1998. b. *AJ* 116, 1169.
Meyer, M et al. 2009.
Meyer, M. J. et al. 2004. *MNRAS* 350, 1195.
Obreschkow, D. et al. 2009a. *ApJ* 703, 1890.
Obreschkow, D. et al. 2009b. *ApJ* 698, 1467.
Richter, O. G. & R. Sancisi. 1994. *A&A* 290, L9.
Roberts, M. S. & M. P. Haynes. 1994. *ARAA* 32, 115.
Saintonge, A. et al. 2017. *ApJS* 233, 22, 22.
Saintonge, A. 2007. *AJ* 133, 2087.
Springel, V. 2005. *MNRAS* 364, 1105.
Stevens, A. R. H. & T. Brown. 2017. *MNRAS* 471, 447.
Taga, M. & M. Iye. 1998. *MNRAS* 299, 1132.
Tamburro, D. et al. 2009. *AJ* 137, 4424.
Tifft, W. G. & W. J. Cocke. 1988. *ApJS* 67, 1.
Wang, J. et al. 2011. *MNRAS* 412, 1081.
Wang, J. et al. 2016. *MNRAS* 460, 2143.
Weinberg, M. D. 1998. *MNRAS* 299, 499.
Westmeier, T. et al. 2014. *MNRAS* 438, 1176.
Wilcots, E. M. & M. K. M. Prescott. 2004. *AJ* 127, 1900.
Yurin, D. & V. Springel. 2014. *MNRAS* 444, 62.
Zaritsky, D. & H.-W. Rix. 1997. *ApJ* 477, 118.

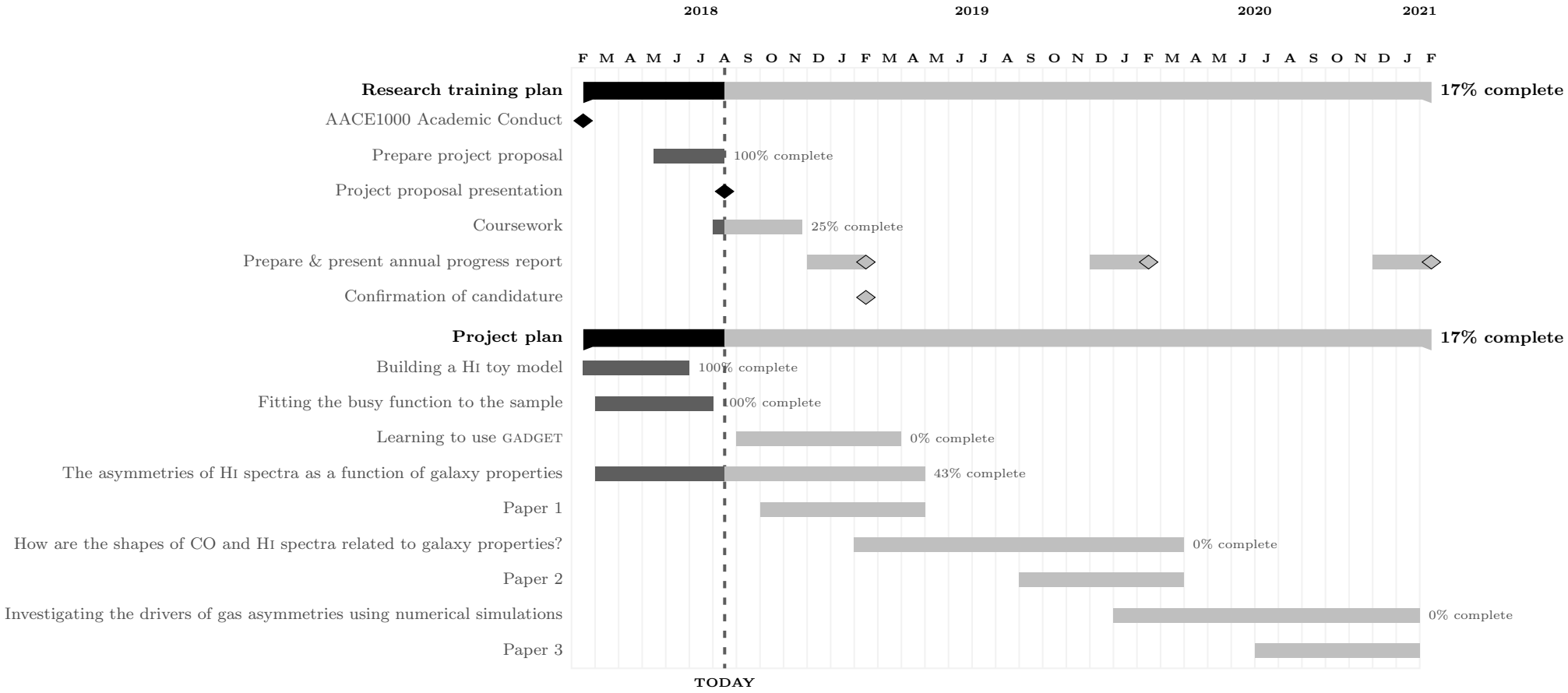

Figure 9: Research Training and Project Plan.